RSC Advances

PAPER

View Article Online
View Journal | View Issue

Cite this: *RSC Adv.*, 2017, **7**, 54039

Polyethylenimine-functionalized cellulose aerogel beads for efficient dynamic removal of chromium(VI) from aqueous solution†

Dong-Mei Guo,[a] Qing-Da An,[*a] Zuo-Yi Xiao,[a] Shang-Ru Zhai[*a] and Zhan Shi[b]

For the highly effective removal of hexavalent chromium from aqueous solutions, a new polyethylenimine (PEI) grafted porous adsorbent, a cellulose@PEI aerogel (CPA-2) composite, was synthesized through a glutaraldehyde crosslinking reaction between the amine groups of PEI and the hydroxyl groups of cellulose. The physicochemical properties of this new adsorbent were characterized by FT-IR, SEM, EDX, XPS, *etc.*, and the modification of grafting with PEI was demonstrated by FT-IR, EDX and XPS analyses. The effects of pH, contact time, initial concentration and PEI content on Cr(VI) sorption were systematically investigated. Experimental data were well described by the Freundlich isotherm and the pseudo-second-order model in a batch system, demonstrating that chemisorption was the rate-controlling factor for Cr(VI) removal with CPA-2. Furthermore, the experimental maximum adsorption capacity of CPA-2 was 229.1 mg g^{-1}, which was around 12 times higher than that of cellulose aerogel (CA) (18.7 mg g^{-1}). The Thomas model was well fitted to the breakthrough curves of adsorption processes under different fixed-bed conditions. Above all, the exhausted bead-like adsorbent could be easily separated and regenerated without significant loss of adsorption capacity. Accordingly, this new composite material should be a promising sorbent for sewage disposal, with advantages of high performance, low-cost, biodegradability and excellent reusability.

Received 6th September 2017
Accepted 18th November 2017

DOI: 10.1039/c7ra09940a

rsc.li/rsc-advances

1. Introduction

With the rapid development of industrialization and urbanization, water contamination such as heavy metal pollution has led to severe environmental problems, which threaten ecological systems and human health. Chromium, a heavy metal existing generally in sewage, usually originates from industries such as textile dyeing, leather tanning and paper making.[1] There are two valences of chromium in its natural state, which are trivalence and hexavalence, having observable differences in toxicities.[2] Trivalent chromium is an essential trace element that is good for metabolizing sugar, protein and fat (the quantity demanded is 50–200 mg a day).[3] Nevertheless, hexavalent chromium, which is highly soluble and mobile in aqueous media, exerts toxicity, carcinogenicity and mutagenicity to humans and animals because of its strong oxidizing properties.[4,5] Nowadays, the U.S. Environmental Protection Agency (EPA) Guidelines give a maximum value of chromium in potable water, namely 0.05 mg L^{-1}.[6] Hence, it is an important issue to remove Cr(VI) from chromium-polluted water to weaken the grave impact of Cr(VI) on human health.

Numerous methods, including photocatalysis,[7] membrane process,[8] adsorption,[9,10] electrochemical treatment[11] and so forth, have been used to remove Cr(VI) from wastewater. Nevertheless, most of these strategies have associated defects which more or less limit their practical application to sewage disposal, for instance, high cost produced by operating, poor efficacy, generation of a toxic sludge and secondary pollutants and so on. By contrast, adsorption is regarded as a simple and cost effective method for the separation of chromium from aqueous solutions, because of the simplicity of design, environmental friendliness, low cost, high efficiency and reusability of adsorbents.[12]

Up to now, a variety of adsorbents, such as graphene,[13] biomass,[14] activated carbon,[3] mineral,[15,16] *etc.*, have been developed to dispose Cr(VI). Amongst them, using low-cost biomass as adsorbent to remove Cr(VI) has received great attention, such as rice husk,[17] cellulose,[18] lignin,[19] sodium alginate[20] and chitosan.[21] Among these materials, cellulose has received increasing attentions owing to its properties which contain inexpensive, abundant, non-toxic, low weight, renewable and biodegradable. There are many –OH groups on the surface of cellulose that can provide some adsorption capacity.

[a]*Faculty of Light Industry and Chemical Engineering, Dalian Polytechnic University, Dalian 116034, China. E-mail: anqingdachem@163.com; zhaisrchem@163.com*
[b]*State Key Laboratory of Inorganic Synthesis and Preparative Chemistry, College of Chemistry, Jilin University, Changchun 130012, China*

† Electronic supplementary information (ESI) available. See DOI: 10.1039/c7ra09940a

However, previous powdery cellulose-based adsorbents are difficult to be separated from sewage, usually employing energy-consuming processes like filtration or centrifuging.[22] To address this issue, the preparation of micrometer-sized cellulose aerogel beads might be an alternative way to solve this bottleneck problem. Moreover, as a result of the low activity of –OH, the adsorption capacity of pure cellulose is little. Hence, surface modification of cellulose materials with more functional groups to significantly enhance the adsorption ability of adsorbent has attracted more and more attentions within the last decades.

Some effective groups such as carbonyl group,[23] carboxyl group[24] and amino group[25,26] can be grafted onto the surface of cellulose to improve the adsorption capacity. By contrast, amino-functionalized adsorbents exerted excellent properties in removing Cr(VI) ions from effluents.[26] For example, Tian *et al.* reported a composite composed of halloysite and polyethyleneimine to dispose chromium-polluted water, and its maximum adsorbing capacity was 102.5 mg g^{-1}.[27] In addition, Chen *et al.* prepared polyethyleneimine-grafted magnetic nanoparticles to dispose sewage, for which the adsorbing capacity of Cr(VI) reached 175.8 mg g^{-1}.[28] Clearly, polyethylenimine (PEI) whose chain has plenty of primary and secondary amino groups is frequently used to modify sorbents by grafting onto the support materials to improve the adsorption capacity for Cr(VI).[29,30] Given that amino groups are easily protonated under acidic conditions, Cr(VI) could be absorbed on polyethyleneimine-modified adsorbents by electrostatic interaction. However, on account of the high solubility of PEI in aqueous system, it is difficult to recover the polymer when it is directly used to remove Cr(VI) from effluents, limiting the application of PEI. Hence, enhancing the stability and reusability of PEI is another important issue for current studies.

To overcome the shortcomings mentioned above, a new core–shell/bead-like cellulose@PEI aerogel composite was produced by grafting PEI onto the surface of cellulose hydrogel beads using glutaraldehyde (GLA) as cross-linking agent. This method could not only introduce plenty of amino groups to the surface of cellulose, but also increase the mechanical property of cellulose hydrogels. Meanwhile, the separation of cellulose@PEI aerogel beads after adsorbing chromium is very simple, avoiding tedious procedures like filtration or other separation process. Thus, the synthetic sorbent was utilized for removing Cr(VI) from effluents. Adsorption experiments were carried out as a function of contact time, pH, initial Cr(VI) concentration, and more significantly flow rate, inlet concentration of column adsorption to investigate the practical potentiality of such new bead-like aerogel composite under dynamic sorption conditions were conducted out, and possible adsorption mechanism was also investigated thoroughly.

2. Materials and methods

2.1 Materials

PEI (M_w = 600, 99%) and α-cellulose (50 μm) were obtained from Sigma-Aldrich Co., Ltd. Glutaraldehyde solution (50%) was purchased from Tianjin Guangfu Fine Chemical Industry Research Institute, China. Ethyl acetate, chloroform, glacial acetic acid, urea, $K_2Cr_2O_7$, ethanol, LiOH were obtained from Tianjin Kermel Chemical Reagent Corporation, China. *tert*-Butanol and acetone, supplied by Sinopharm Chemical Reagent Co., Ltd, China. Deionized water was used throughout this work. All the chemicals were used as-received without any further treatment.

2.2 Synthesis of cellulose@PEI aerogel beads

The schematic of synthesizing cellulose@PEI aerogel beads is shown in Scheme 1. Solvent system of LiOH/urea/H_2O (4.6 : 15 : 80.4 w/w) was prepared at first. Afterwards, a certain amount of α-cellulose (4 g) was dispersed into 100 g solvent mixture under violent stirring for 2 h at room temperature. After that, mixed solution was cooled to −18 °C for 2 h, and then dissolved at ambient temperature under magnetic stirring to obtain a transparent cellulose solution. Cellulose hydrogel beads were prepared by added dropwise of the cellulose solution (4%, w/w) into a coagulation bath of ethyl acetate/chloroform/glacial acetic acid (3 : 3 : 1 v/v) for 10 min, and then the obtained cellulose beads were transferred into glacial acetic acid solution (1%, w/w) for 24 h for the purpose of solidification. Ethyl acetate/chloroform/glacial acetic acid solution could be collected and reused. Afterwards the cellulose hydrogel beads were separated and repeatedly washed with water to remove extra chemical reagents.

The cellulose hydrogel beads and a certain amount of PEI were then added into 60 mL deionized water stirring for 1 h to make it totally dispersed. Next, 40 mL aqueous glutaraldehyde solution as crosslinking agent was put into the hybrid and agitated for 2 h to obtain core–shell/bead-like cellulose@PEI hydrogel beads,[31] followed by washing with deionized water to wash away the residual PEI and glutaraldehyde. The absorbed water in cellulose hydrogel beads was exchanged with ethanol which was then replaced by the *tert*-butanol. Lastly, cellulose@PEI hydrogels were frozen at −50 °C for 12 h, and subjected to freeze-drying at −50 °C for 12 h. By varying the amount of PEI (1, 1.5, 2, 2.5 and 3 g), five samples of cellulose@PEI aerogel were generated and coded as CPA-1, CPA-1.5, CPA-2, CPA-2.5 and CPA-3, respectively.

Pure cellulose aerogel (CA) was prepared by the same method as a control sample. Moreover, the *tert*-butanol replacement prior to freeze-drying was conducted out for the sake of ensuring admirable voids and three-dimensional network structure of the aerogel, which would be demonstrated by the characterization analysis as follows.

2.3 Characterization

The FT-IR spectra were measured on Nicolet 5700 FT-IR spectroscope (Nicolet, USA) between 4000 and 500 cm^{-1} using the KBr pellet technique. The scanning electron microscopy (SEM) and the energy dispersive X-ray spectroscopy (EDX) images were carried out on a Hitachi S-4800 SEM instrument (Hitachi, Japan) to investigate the morphology and structural of composites. X-ray photoelectron spectra (XPS) were studied by an ESCALAB MKII X-ray photoelectron spectrometer. It is worth mentioning

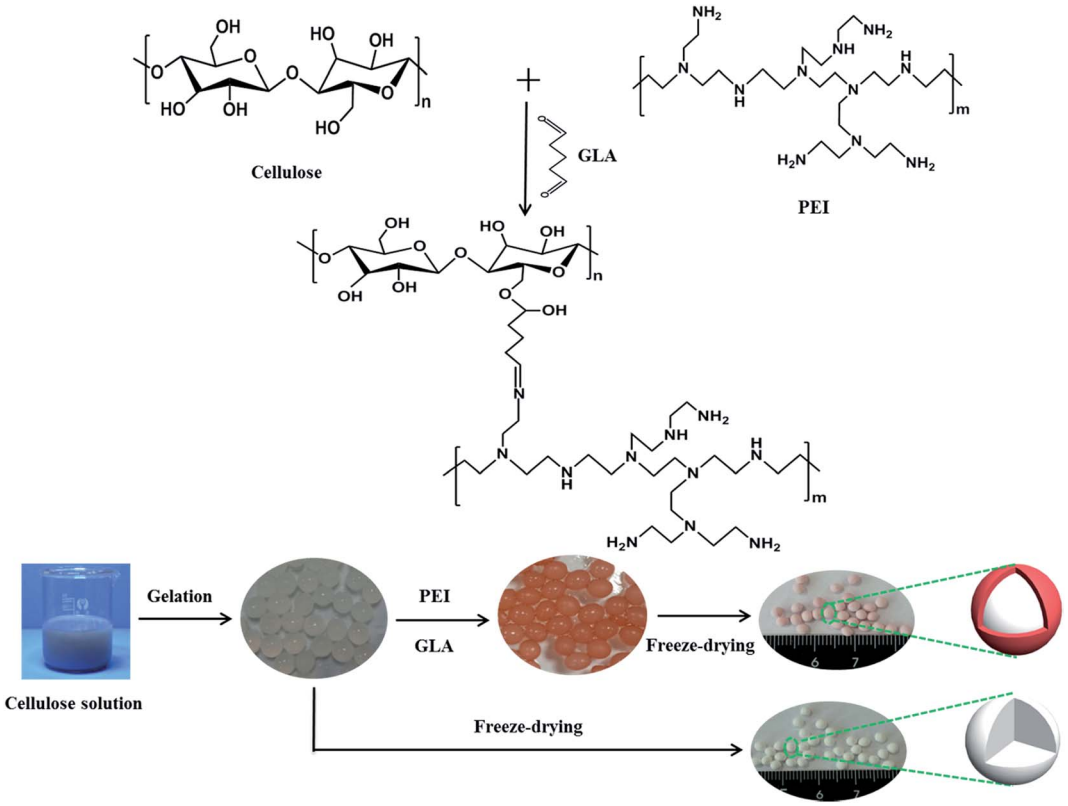

Scheme 1 The synthesis route to prepare cellulose aerogel beads and core–shell cellulose@PEI aerogel beads.

that EDX and XPS were used to confirm the chemical modification process and reveal the adsorption mechanism. The specific surface area and pore diameter were obtained by using a surface area analyzer (Quantachrome Autosorb NOVA2200e, USA). The concentration of Cr(VI) was measured by a UV-vis spectrophotometer (UV-754N Shanghai, China). All pH values were evaluated by Delta320 digital pH meter (Mettler-Toledo, Switzerland). Moreover, the surface zeta potentials of CPA-2 were studied by Malvern Zen 3600 Zetasizer (Malvern Instruments, United Kingdom) under different pH conditions.

2.4 Batch adsorption experiments

A series of batch adsorption experiments including effects of contact time, pH and initial concentration of Cr(VI) were conducted in 50 mL glass conical flasks in which 0.02 g of sorbent was added into 20 mL solution of calculated Cr(VI) concentration by shaking at 180 rpm at 25 °C. Magnetic stirring could ensure the homogeneity of system in adsorption process. Moreover, solution pH was adjusted by using 0.1 M HCl or 0.1 M NaOH. Then residual concentration of Cr(VI) ions was monitored by UV-vis absorption spectrophotometry at maximum absorbance wavelength of 540 nm. And the adsorption capacity at specific times and equilibrium were calculated by the following equations:

$$q_t = \frac{(C_0 - C_t)V}{m} \quad (1)$$

$$q_e = \frac{(C_0 - C_e)V}{m} \quad (2)$$

where q_t (mg g^{-1}) and q_e (mg g^{-1}) are the amount of Cr(VI) adsorbed on cellulose@PEI aerogel beads at time t and equilibrium; C_0, C_t, and C_e (mg L^{-1}) represent the initial, time t, and equilibrium concentration of Cr(VI) solution, respectively; V (mL) represents the volume of solution; m (mg) represents the adsorbent dose.

2.5 Column adsorption experiments

The typical CPA-2 beads with an average size of 3 mm was packed into the fixed-bed column on account of the bead-like structure of cellulose@PEI aerogel beads, by which was favorable for the dynamic adsorption. Fixed-bed column operations were conducted in glass column whose internal diameter and length were 1.2 cm and 10 cm, respectively. The column reactors were packed with 0.590 g CPA-2 at bed depth of 8 cm. Before each experiment, a little gauze was placed at the bottom of fixed-bed reactor to make the sorbent stabilized. The concentrations of Cr(VI) solution fed into the column at a determinate flow rate (1, 2 and 3 mL min^{-1}) by a peristaltic pump were 50 and 75 mg L^{-1}, respectively. The samples flowing out were collected at decided time intervals and measured by UV-vis spectrophotometer. The column experiments were used to investigate the practical application properties of adsorbent. The time of breakthrough appearance and the shape of the breakthrough curve are essential features for confirming the dynamic

response of a fixed-bed column. And the breakthrough curves were drew by ratio of outflow and inlet metal concentration (C_t/C_0) as a function of time. The continuous Cr(VI) uptake process was continued until the exhaustion point ($C_t/C_0 = 0.9$) of the column appeared. The outlet concentration from the fixed bed reaching about 10% of the feed concentration is breakthrough point.

Total adsorbed metal quantity, q_{total} (mg), is equal to the area under the plot of the adsorbed Cr(VI) concentration C_{ad} ($C_{ad} = C_0 - C_t$) (mg L^{-1}) against t (min), could be calculated using:

$$q_{total} = \frac{QS}{1000} = \frac{Q}{1000}\int_{t=0}^{t=t_{total}} C_{ad}\,dt \quad (3)$$

where Q and t_{total} are the volumetric flow rate (mL min^{-1}) and total flow time (min), respectively. S represents the area under the breakthrough curve. The chromium-polluted water treatment capacity V_E was calculated using:

$$V_E = Qt_{total} \quad (4)$$

The maximum capacity of the fixed bed, q_e (mg g^{-1}), was evaluated from eqn (5):

$$q_e = \frac{q_{total}}{X} \quad (5)$$

where X (g) is the weight of adsorbent in the column.

Total amount of Cr(VI) sent to column, W (mg), could be calculated as following:

$$W = \frac{C_0 Qt_{total}}{1000} \quad (6)$$

Total removal (R (%)) was calculated from eqn (6):

$$R = \frac{q_{total}}{W} \times 100 \quad (7)$$

The empty bed contact time (EBCT) is an important parameter. Generally speaking, the V_E is increased with the increase in EBCT. The EBCT in the column can be described as following:

$$\text{EBCT(min)} = \frac{\text{bed volume}}{Q} \quad (8)$$

3. Results and discussion

3.1 Batch adsorption experiments

3.1.1 Effect of the pH. As we all know, the pH value of liquid waste is a vital factor in removing metal ions, considering the fact that it could not only influence the charge density of sorbent but also determine Cr(VI) speciation in effluents. Different pH values of 1 to 8 were applied for the purpose of researching the optimal pH for metal ions adsorption process over cellulose@PEI aerogel beads with original Cr(VI) concentrations of 100 mg L^{-1}. Adsorption processes were enforced at ambient temperature and stirring continued for 24 h. The

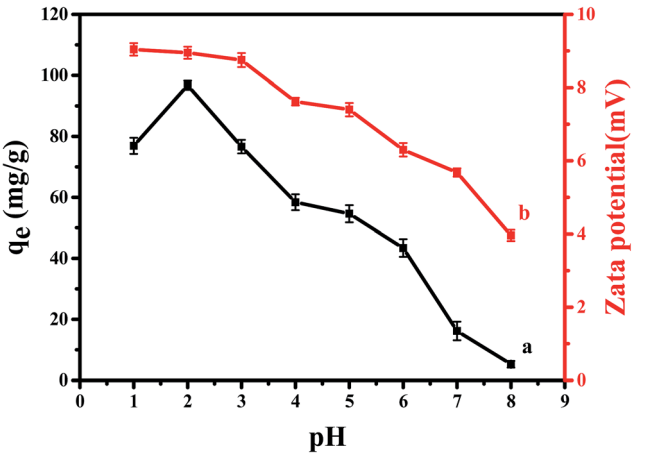

Fig. 1 (a) Effect of pH on the adsorption of Cr(VI) on CPA-2; (b) zeta potential analysis at different solution pH onto CPA-2.

results in Fig. 1a illustrated that the adsorbing capacity of Cr(VI) increased with the increase of pH from 1 to 2, and then decreased with increasing pH from 2 to 8. Clearly, the maximum adsorbing capacity of Cr(VI) was 96.8 mg L^{-1} at pH = 2, for which can be selected for the subsequent experiments.

The impact of solution pH on chromium uptake could be elucidated by the surface charge of sorbent and the degree of ionization of adsorbate. Therefore, the surface charges of CPA-2 were measured at various pH values. From Fig. 1b, it should be noted that cellulose@PEI composite was positively charged and zeta potential value decreased with increasing pH from 1 to 8. The positive charge could be associated with PEI, which is a cationic polyelectrolyte. There are many $-NH_2$ on cellulose@PEI aerogel that would be protonated to form $-NH_3^+$ in low pH solution, resulting in an electrostatic attraction to negatively charged Cr(VI) ions,[32] which can lead to an increase in adsorption capacity. When the solution pH increased, the degree of $-NH_2$ protonation decreased, making a decrease in surface charge of CPA-2.

In addition, Cr(VI) exists various forms such as H_2CrO_4, $HCrO_4^-$, CrO_4^{2-} and $Cr_2O_7^{2-}$ in water which are associated with solution pH. The dominant forms of Cr(VI) would interconvert from CrO_4^{2-} to $HCrO_4^-$ and $Cr_2O_7^{2-}$ when pH value is lower than 6.5, while pH above 6.5 hexavalent chromium could be transformed as CrO_4^{2-}. In addition, H_2CrO_4 is predominant at pH less than 2.[33] In contrast to CrO_4^{2-}, $Cr_2O_7^{2-}$ has the same charge but double Cr(VI) amount, so does the $HCrO_4^-$ owing to charge balance, making the uptake capacity increased significantly. In other words, increasing the ratio of $HCrO_4^-$ and $Cr_2O_7^{2-}$ would give rise to an improvement of Cr(VI) removal. Moreover, at pH < 2, the existence of H_2CrO_4 could cause reduction of electrostatic attraction between CPA-2 and Cr(VI). Consequently, the optimal pH value appeared at 2, which was consistent with previous work.[28]

3.1.2 Adsorption isotherms. Adsorption isotherms are extremely important in the optimization of adsorbents, due to the fact that it not only can evaluate the adsorbability of adsorbent, but also reveal the interaction between adsorbate and sorbent. Accordingly, the adsorption isotherms were

investigated with CA, CPA-1, CPA-1.5, CPA-2, CPA-2.5 and CPA-3 over the initial Cr(VI) concentration range of 10–700 mg L^{-1} at ambient temperature for 24 h. As shown in Fig. S1,† with the increase of equilibrium Cr(VI) concentration, sorption capacities of all the composites increased, manifesting that initial concentration of Cr(VI) ions played an important role in affecting the adsorption capacity. Moreover, the maximum adsorption capacity increased with increasing PEI content because of the increased number of active sites contributed by PEI molecules. That is, the more PEI used in the synthesis process, the more $-NH_2$ would bond on the surface of the cellulose, improving the adsorbing capacity. Nevertheless, when the amount of PEI increased from 2 to 3 g, there was a little increase of Cr(VI) adsorption on the surface of cellulose@PEI beads. In consideration of the adsorption ability and cost effectiveness in practical applications, CPA-2 was determined as the optimal sorbent for following experiments. Besides, when the original concentration was lower than 125 mg L^{-1}, the residual concentration of chromium after removal by CPA-2 was inappreciable.

Langmuir and Freundlich models, two famous types of isotherm models, were used to simulate the equilibrium data. Langmuir model is based on the assumption that the adsorption process is monolayer sorption on a homogeneous sorption surface and all sorption sites are almost identical. Hence, it can reach saturation. Nevertheless, Freundlich isotherm model is used to characterize multilayer adsorption.[34] These two models are represented as:

Langmuir:

$$q_e = \frac{q_m K_l C_e}{1 + K_l C_e} \quad (9)$$

$$R_l = \frac{1}{1 + K_l C_0} \quad (10)$$

Freundlich:

$$q_e = K_f C_e^{\frac{1}{n}} \quad (11)$$

where q_e and C_e are the adsorption capacity (mg g^{-1}) and Cr(VI) concentration (mg L^{-1}) at equilibrium, respectively. C_0 represents the initial concentration (mg L^{-1}) and q_m represents the maximum adsorbing capacity (mg g^{-1}). K_l represents Langmuir constant (L mg^{-1}) related to the adsorption energy, K_f and n are related to the capacity and intensity of the adsorption, respectively, and R_l is Langmuir constant separation factor. The non-lineared adsorption isotherm curves were presented in Fig. 2, and related parameters of the adsorption isotherm models were summarized in Table 1. The correlation coefficient R^2 of Freundlich model of all cellulose@PEI composites were higher than that of Langmuir model, suggesting that heterogeneous coverage of target hexavalent chromium on the surface of cellulose@PEI beads. The correlation to the Freundlich model can support the existence of electrostatic interaction between Cr(VI) and functional groups of CPA-2.[35] It is worth mentioning that the correlation coefficient R^2 of Freundlich model and Langmuir model were close. To further analyze the non-lineared adsorption isotherm curves of Cr(VI), isotherm curves could fit well with Langmuir model when the concentration is low. This phenomenon may be attributed to the electrostatic attraction between protonated $-NH_3^+$ and Cr(VI) anions. If Cr(VI) concentration is low, the surface active sites would dominate the adsorption, making sorption process followed monolayer sorption. When the concentration is higher, the adsorption process followed multilayer adsorption. Interestingly, the adsorption isotherm of chromium onto CA fitted better with Langmuir model, implying a monolayer adsorption process.

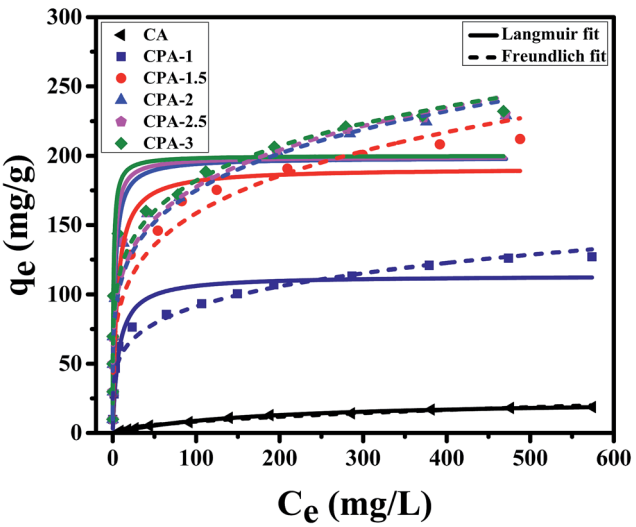

Fig. 2 Langmuir and Freundlich isotherm models of Cr(VI) removal using CA, CPA-1, CPA-1.5, CPA-2, CPA-2.5 and CPA-3.

Table 1 Langmuir and Freundlich models parameters for Cr(VI) adsorption on cellulose@PEI beads prepared with varied PEI amount

	Langmuir isotherm				Freundlich isotherm		
samples	q_m (mg g^{-1})	K_l (L mg^{-1})	R_l	R^2	K_f (mg g^{-1})	n	R^2
CA	24.39	0.0056	0.2033–0.9470	0.9958	0.7979	1.9742	0.9767
CPA-1	113.66	0.1421	0.0099–0.4131	0.9152	34.5086	4.7259	0.9640
CPA-1.5	191.06	0.1946	0.0073–0.3394	0.9298	55.7269	4.4056	0.9443
CPA-2	198.71	0.4167	0.0034–0.1943	0.8944	68.3574	4.8976	0.9537
CPA-2.5	199.19	0.6109	0.0023–0.1407	0.9002	70.0826	4.9548	0.9393
CPA-3	200.16	0.9270	0.0014–0.0887	0.9055	77.3620	5.3802	0.9345

From the Freundlich model, it can be observed that adsorption intensity $n > 1$, which indicated that the adsorption is favorable. Moreover, the values of R_l were between 0 and 1, revealing the favorable adsorption of Cr(VI) by cellulose@PEI composites, too.

In addition, the q_m value of CPA-2 for chromium acquired from Langmuir model was 198.7 mg g^{-1}, while the experimental maximum sorption capacity of CPA-2 was 229.1 mg g^{-1}, which was around 12 times higher than the sorption capacity of Cr(VI) on CA (18.7 mg g^{-1}), manifesting that the adsorption capacity was observably enhanced by the modification of PEI and considerably higher than other previously reported adsorbents. The q_m values of CPA-2 and other adsorbents under similar conditions were summarized in Table 2. The CPA-2 which could be separated from effluents easily had a fairly greater adsorption capacity than those previously reported adsorbents, indicating that CPA-2 has a good potential in the decontamination of chromium-polluted water.

3.1.3 Adsorption kinetics. The effect of contact time on the CPA-2 towards Cr(VI) ions at two initial concentrations (50 and 100 mg L^{-1}) was depicted in Fig. 3. With the increase of concentration (50 to 100 mg L^{-1}), the time needed to reach equilibrium increased from 100 to 300 min. The adsorption capacity of CPA-2 increased rapidly and reached almost 90% in first stage, which took 60–180 min depending on concentrations of Cr(VI), then the growth trend reduced until the uptake capacity reached saturation. This result suggested that CPA-2 could rapidly adsorb Cr(VI) from sewage attributing to the properties of the cellulose@PEI composite. Firstly, the porous structure of cellulose aerogel and the strong metal chelating ability of amino group were favorable to the contaction of metal ions and active sites.[36] Secondly, because of the large molecular weight of PEI, the active amino group was only modified on the surface of material.[37]

As is well known that pseudo-first-order model was based on the assumption that the adsorption process is primarily controlled by internal diffusion process, while the pseudo-second-order kinetic model was based on the assumption that the adsorption process is mainly controlled by chemisorption of adsorbate molecules on active sites. The kinetic data of Cr(VI) on CPA-2 were fitted by pseudo-first-order and pseudo-second-order rate equations,[38] which were expressed as:

Table 2 Comparison of the CPA-2 adsorbent with other materials

Adsorbents	q_{max} (mg g^{-1})	Ref.
PEI grafted γ-Fe_2O_3@Fe_3O_4 nanoparticles	78.1	48
Activated carbon	15.5	49
Quaternized rice hulls	32.3	50
Amino-functionalized mesoporous silica	118.6	51
PEI immobilized acrylate-based magnetic beads	140.6	28
PEI–HNTs	102.5	27
Amino-functionalized magnetic cellulose	171.5	52
Graphene oxide functionalized with magnetic	67.7	53
PEI–MNPs	175.8	31
CPA-2	229.1	This work

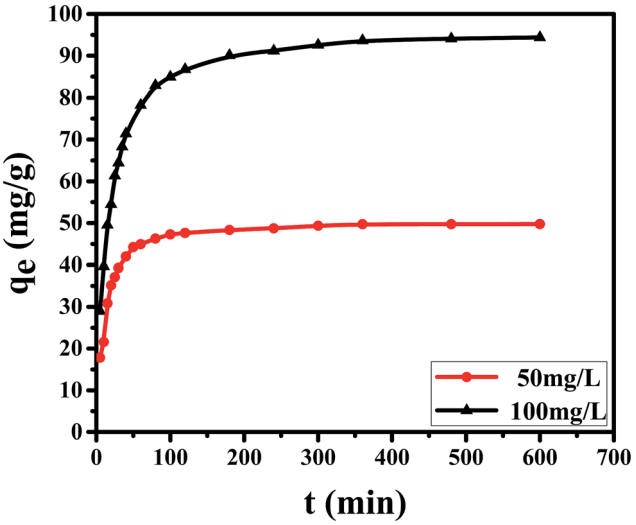

Fig. 3 Influence of contact time on Cr(VI) removal by CPA-2.

$$\ln(q_e - q_t) = \ln q_e - K_1 t \quad (12)$$

$$\frac{t}{q_t} = \frac{1}{K_2 q_e^2} + \frac{t}{q_e} \quad (13)$$

where q_e (mg g^{-1}) and q_t (mg g^{-1}) represent the amount of Cr(VI) adsorbed at equilibrium and time t, and K_1 (min^{-1}) and K_2 (g mg^{-1} min^{-1}) are pseudo-first-order and pseudo-second-order rate constant, respectively. The adsorption kinetic model curves were illustrated in Fig. 4a and b, and corresponding kinetic parameters from both models were listed in Table 3. As indicated in Table 3, the adsorption of Cr(VI) ions by CPA-2 was considerably better fitted with the pseudo-second-order kinetic model than the pseudo-first-order kinetic model. The values of R^2 for the pseudo-second-order kinetic model were 0.9999 for different original concentrations, and the calculated q_e values ($q_{e,cal}$) of this model agreed with the experimental values (Table 3). Based on the assumptions of the pseudo-second-order model, chemisorption between the Cr(VI) ions and active sites of CPA-2 was considered to be the rate controlling step in this study.

3.1.4 Effect of coexisting ions and TOC. The effluent generally contains a certain concentration of coexistent cations and anions which could affect the adsorption process of Cr(VI).[3] As is well known that Cr(VI) exists in the form of anions in aqueous solution, and the adsorption of Cr(VI) occurs on the CPA-2 surface by electrostatic interactions. Therefore, the cations would not influent the adsorption process of chromium.

By using 20 mg dosage of CPA-2 and 50 mg L^{-1} (20 mL) as initial Cr(VI) concentration at pH 2, the adsorption experiments was performed by different concentrations of co-existing anions (Cl^-, NO_3^-, F^-, PO_4^{3-} and SiO_3^{2-}) and TOC (Acid Red 94). The results were depicted in Fig. 5. As shown in the Fig. 5a, the Cl^-, NO_3^- and F^- had no remarkable competitive influence on the adsorption of Cr(VI) onto CPA-2. Nevertheless, the removal capacity for Cr(VI) decreased rapidly with the increase of the concentration of PO_4^{3-} and SiO_3^{2-}. When the concentration of PO_4^{3-} and SiO_3^{2-} increased from 200 to 2000, the q_t of Cr(VI)

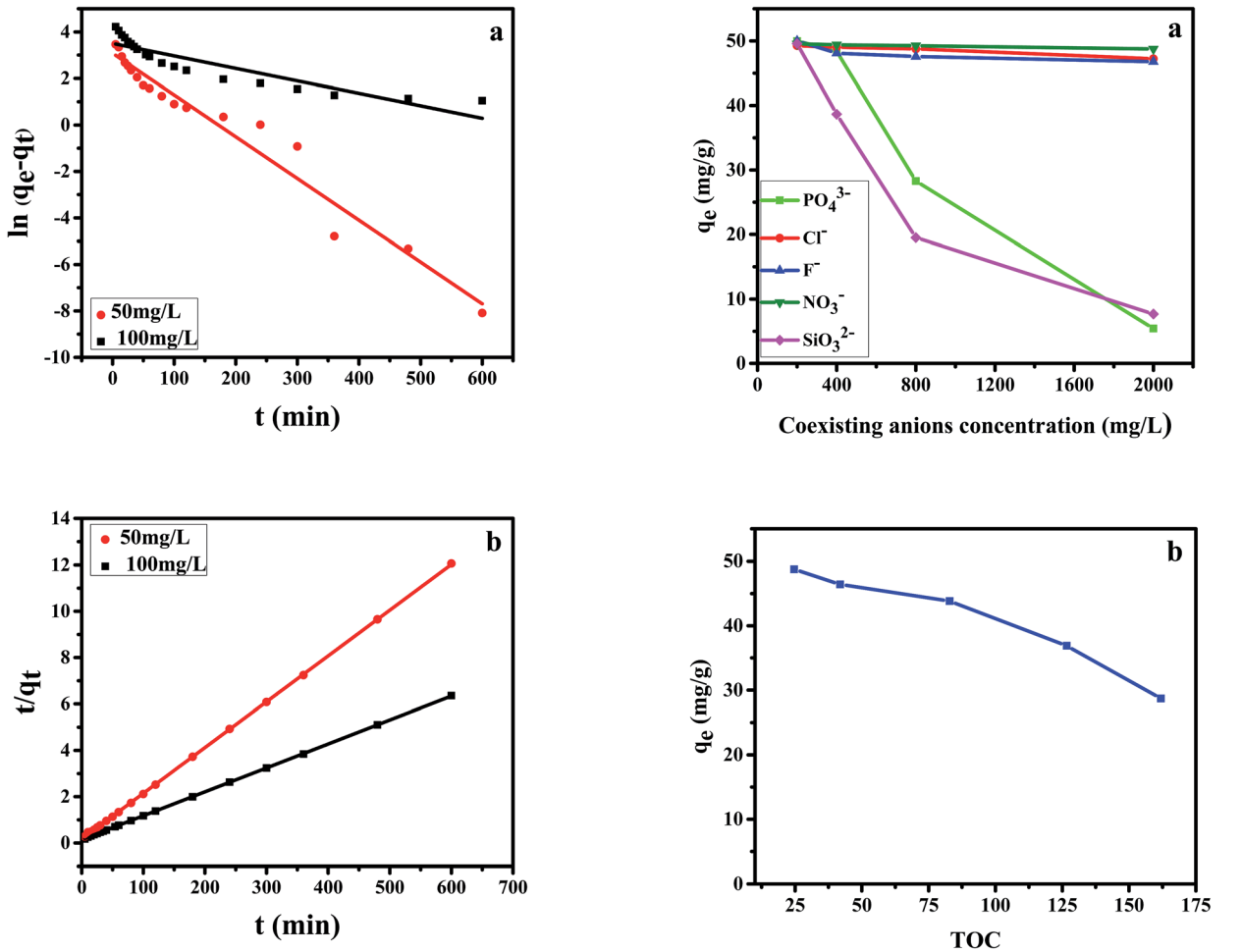

Fig. 4 The (a) pseudo-first-order, (b) pseudo-second-order kinetic model of Cr(VI) removal on the CPA-2.

Fig. 5 Effect of coexisting ions and TOC on the adsorption of Cr(VI) by CPA-2.

decreased from 49.99 to 5.41 mg L^{-1} and 49.59 to 7.67 mg L^{-1}, respectively. On the one hand, the coexisting PO_4^{3-} and SiO_3^{2-} which can produce HPO_4^{2-}, $HSiO_3^{-}$ and OH^{-} under hydrolytic process changed the pH of aqueous solution. The increased pH exerted distinct inhibitory effect on the chromates adsorption. On the other hand, competition adsorption could be used to explain the results, too. The Cl^{-}, NO_3^{-} and F^{-} are monovalent anions, which have little competition with Cr(VI) ions for the active sites on CPA-2. By contrast, PO_4^{3-} and SiO_3^{2-} are multivalent anions. There are distinct competitive effects between the multivalent anions and Cr(VI). Those results were consistent with the previous works.[3,21] As can be seen from the Fig. 5b, the uptake capacity of Cr(VI) decreased with the increase of TOC. When the concentration of TOC increased from 24.66 to 161.92, the removal capacity of Cr(VI) decreased from 48.75 to 32.71 mg L^{-1}. The Acid Red 94 is anionic dye that can compete active adsorption sites with Cr(VI) ions, resulting in the decrease of removal capacity.

3.1.5 Effect of real wastewater. The effect of real wastewater on the CPA-2 towards Cr(VI) ions in three initial concentrations (50, 100 and 200 mg L^{-1}) solution which were prepared by dissolving $K_2Cr_2O_7$ in deionized water and filtered real wastewater was depicted in Fig. 6. When the initial concentration was 50 mg L^{-1}, the adsorption capacity of deionized water and real wastewater were 49.65 and 48.14 mg L^{-1}, respectively. With the

Table 3 Kinetic parameters for Cr(VI) adsorption by CPA-2 beads at different initial concentrations

		Pseudo-first-order			Pseudo-second-order		
C_0 (mg L^{-1})	$q_{e,exp}$ (mg g^{-1})	K_1	$q_{e,cal}$ (mg g^{-1})	R^2	K_2	$q_{e,cal}$ (mg g^{-1})	R^2
50	49.73	0.0180	21.83	0.9570	0.0023	50.63	0.9999
100	96.76	0.0054	33.24	0.8109	0.0007	96.81	0.9999

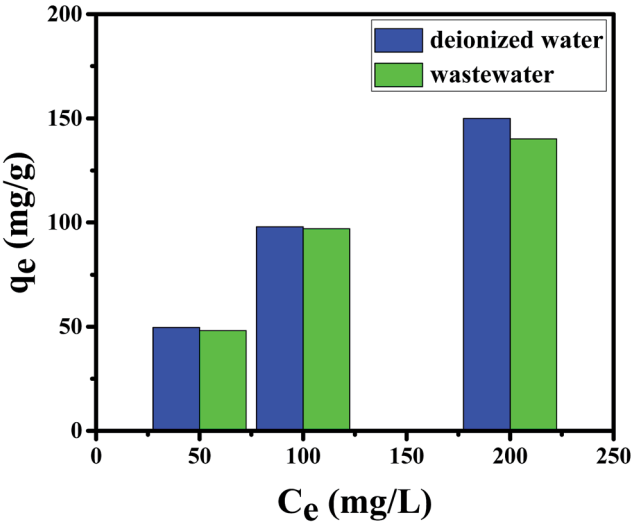

Fig. 6 The effect of deionized water and wastewater on the removal of Cr(VI).

increase of initial concentrations the adsorption capacities increased, and the sorption capacities of real wastewater slightly lower than deionized water. Although the adsorption capacities were reduced to some extent, the removal capacities of chromium were still remain high. The successful adsorption of real wastewater which include many kinds of ions and organic compounds also indicates that coexisting ions and TOC had no remarkable influence on the adsorption of Cr(VI) onto CPA-2.

3.2 Dynamic column adsorption testing

3.2.1 Effect of flow rate. Three different flow rates of 1, 2 and 3 mL min^{-1} were used to investigate the effect of the flow rate on the breakthrough curves of Cr(VI) with a constant bed depth of 8 cm and inlet Cr(VI) concentration of 50 mg L^{-1} at pH 2. The breakthrough curves at various flow rates were shown in Fig. 7a and all parameters were presented in Table 4, where it can be seen that the steepness of the breakthrough curves increased with the flow rate increasing. Breakthrough time reaching saturation was occurred more quickly with an increase in the flow rate, as well. The possible reasons behind these are that Cr(VI) ions have longer time to touch with binding sites on CPA-2 at a low rate of influent, resulting in a greater adsorption of Cr(VI) in fixed bed; on the contrary, during using the higher flow rate, the mass transfer rate tend to increase and the amount of Cr(VI) adsorbed on fixed-bed column increased, leading to the saturation point occurred rapidly. Thus, for lower flow rate whose contact time is longer could visibly improve the Cr(VI) removal efficiency in practical applications.

3.2.2 Effect of inlet Cr(VI) concentration. Initial concentration of Cr(VI) has important influence on the breakthrough curve owing to stronger driving force is supplied for Cr(VI) removal by higher Cr(VI) concentration during the adsorption process.[39] The sorption breakthrough curves obtained by varying feed Cr(VI) concentration from 50 to 75 mg L^{-1} at

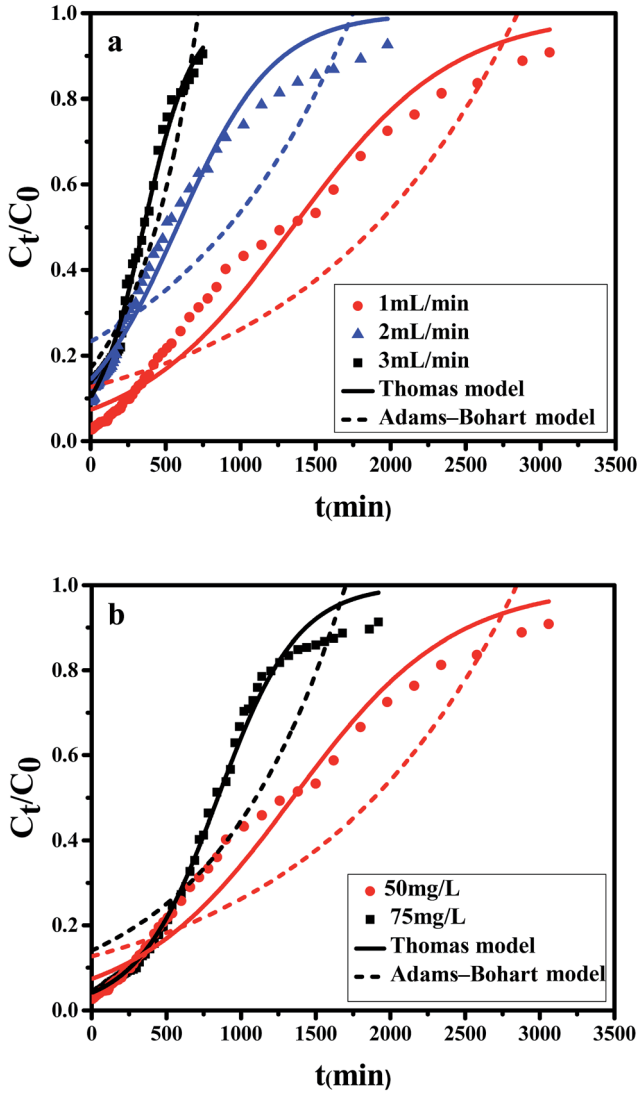

Fig. 7 Experimental and predicted breakthrough curves of Cr(VI) removal by CPA-2 using fixed-bed (a) different flow rates (C_0 = 50 mg L^{-1}, H = 8 cm, pH = 2, T = 298 K); (b) different initial Cr(VI) concentrations (Q = 1 mL min^{-1}, H = 8 cm, pH = 2, T = 298 K).

1 mL min^{-1} flow rate, pH 2 and 8 cm bed height were given in Fig. 7b. Table 4 listed the calculated parameters of Cr(VI) removal by CPA-2 at different influent concentrations.

It is shown that the slope of breakthrough curve increased with the inlet Cr(VI) concentration increasing. At lower feed concentration, breakthrough curve was dispersed and saturation point occurred slowly because of the weaker driving force in the mass transfer process. As initial concentration increased, a steeper breakthrough curve was obtained which could be explained by the condition that more hexavalent chromium could be available to bind with the active sites at higher concentration.

3.2.3 Dynamic column adsorption modeling. For the purpose of describing the dynamic behavior of fixed-bed column and scaling up it for industrial applications, Adams–Bohart and Thomas models were employed to fit breakthrough curves,[40] and the calculated parameters of different operating

Table 4 Column adsorption parameters for Cr(VI) by CPA-2

Q (mL min^{-1})	C_0 (mg L^{-1})	pH	W (mg)	t_{total} (min)	q_{total} (mg)	q_e (mg g^{-1})	R (%)
1	50	2	153	3060	70.48	119.46	46.07
2	50	2	198	1980	36.80	62.37	18.58
3	50	2	112.5	750	17.44	29.56	15.50
1	75	2	144	1920	66.62	112.91	46.26

conditions were listed in Table 5. The Adams–Bohart model assumes a rectangular isotherm with a quasi-chemical rate expression. Adams–Bohart model which is established on the basis of the surface reaction theory assumes that the balance is not instantaneous, and the adsorption rate depends on the amount of residual adsorbate and adsorbent adsorption capacity. The Thomas model base on Langmuir equation with a pseudo second-order rate expression and assumes that the ideal model without axial diffusion, which can be used to estimate the equilibrium adsorption and adsorption rate constant. The predicted and experimental breakthrough curves of Cr(VI) uptake by CPA-2 at different flow rate and inlet concentration were shown in Fig. 7.

The Thomas model is one of the most ecumenically applied models for continuous flow systems,[41] which can be expressed as:

$$\frac{C_t}{C_0} = \frac{1}{1 + e^{\frac{K_T q_0 M}{Q} - K_T C_0 t}} \quad (14)$$

in which C_0 and C_t are the feed and outlet Cr(VI) concentration (mg L^{-1}), K_T represents Thomas model constant (L min^{-1} mg^{-1}), q_0 represents the removal capacity (mg g^{-1}), Q is flow rate (mL min^{-1}) and M is the sorbent mass (g).

The Bohart–Adams model was used to fit the initial part of the breakthrough curve,[42] which was focused on estimating characteristic parameters, such as N_0 and K_{AB}, and the model was given as follows:

$$\frac{C_t}{C_0} = e^{K_{AB} C_0 t - K_{AB} N_0 \frac{Z}{F}} \quad (15)$$

in which K_{AB} represents the kinetic constant (L min^{-1} mg^{-1}), N_0 represents the maximum uptake capacity (mg mL^{-1}), Z represents bed depth (cm) and F represents the linear speed (cm min^{-1}).

As can be seen from the Table 5, for the Thomas model, the uptake capacity (q_0) decreased with the increase of feed concentration or flow rate of Cr(VI), while the value of K_T increased. Therefore, lower flow rate and inlet concentration would increase the removal of Cr(VI) on the CPA-2 beads. For the Adams–Bohart model, the values of K_{AB} increased with inlet concentration or flow rate increasing, while the values of N_0 decreased with influent concentration or flow rate increasing. These results represented that the system kinetics was controlled by external mass transfer in the initial stage of Cr(VI) adsorption. By comparing the correlation coefficients (R^2) obtained from all the dynamic models, the correlation coefficient values generated from the Thomas model were much higher than those from the Adams–Bohart model. It was concluded that the Thomas model was more suitable for the processes of Cr(VI) removal on the CPA-2 under different fixed-bed conditions, while the Bohart–Adams model could be used to fit the initial part of the breakthrough curve.

3.3 Characterization of resultant materials

3.3.1 SEM and EDX analysis. The morphology and structure of the CA, CPA-2 and after Cr(VI) adsorption on CPA-2 (CPA-2-Cr) were investigated by SEM, and Fig. 8a–d showed the desirable three-dimensional network structure of these composites. From the photos, it was observed that PEI observably constringed the pore size of cellulose aerogel, which probably due to PEI molecules grafted on cellulose and partially occupied the interspace among cellulose molecules. However, comparison of the SEM images revealed that the network structure of cellulose aerogel beads has not been damaged by the introduction of PEI and the uptake of Cr(VI).

Additionally, EDX mapping were used to reveal the element type and content of cellulose aerogel beads. As can be seen, C and O elements existed in CA beads (Fig. 8e), while N element

Table 5 Parameters of Adams–Bohart and Thomas models analyzed for Cr(VI) removal by CPA-2 in column adsorption

	Thomas model			Adams–Bohart model		
Parameter	K_T (L min^{-1} mg^{-1})	q_0 (mg g^{-1})	R^2	K_{AB} (L min^{-1} mg^{-1})	N_0 (mg L^{-1})	R^2
Flow rate (mL min^{-1})						
1	3.760×10^{-5}	114.2	0.9672	4.738×10^{-9}	48 169 484	0.8202
2	6.180×10^{-5}	97.8	0.9688	8.407×10^{-9}	38 308 064	0.7666
3	1.228×10^{-4}	89.9	0.9907	6.56×10^{-8}	8 921 867	0.9143
Initial concentration (mg L^{-1})						
50	3.760×10^{-5}	114.2	0.9672	4.738×10^{-9}	48 169 484	0.8202
75	4.973×10^{-5}	107.5	0.9938	7.986×10^{-9}	27 184 079	0.8121

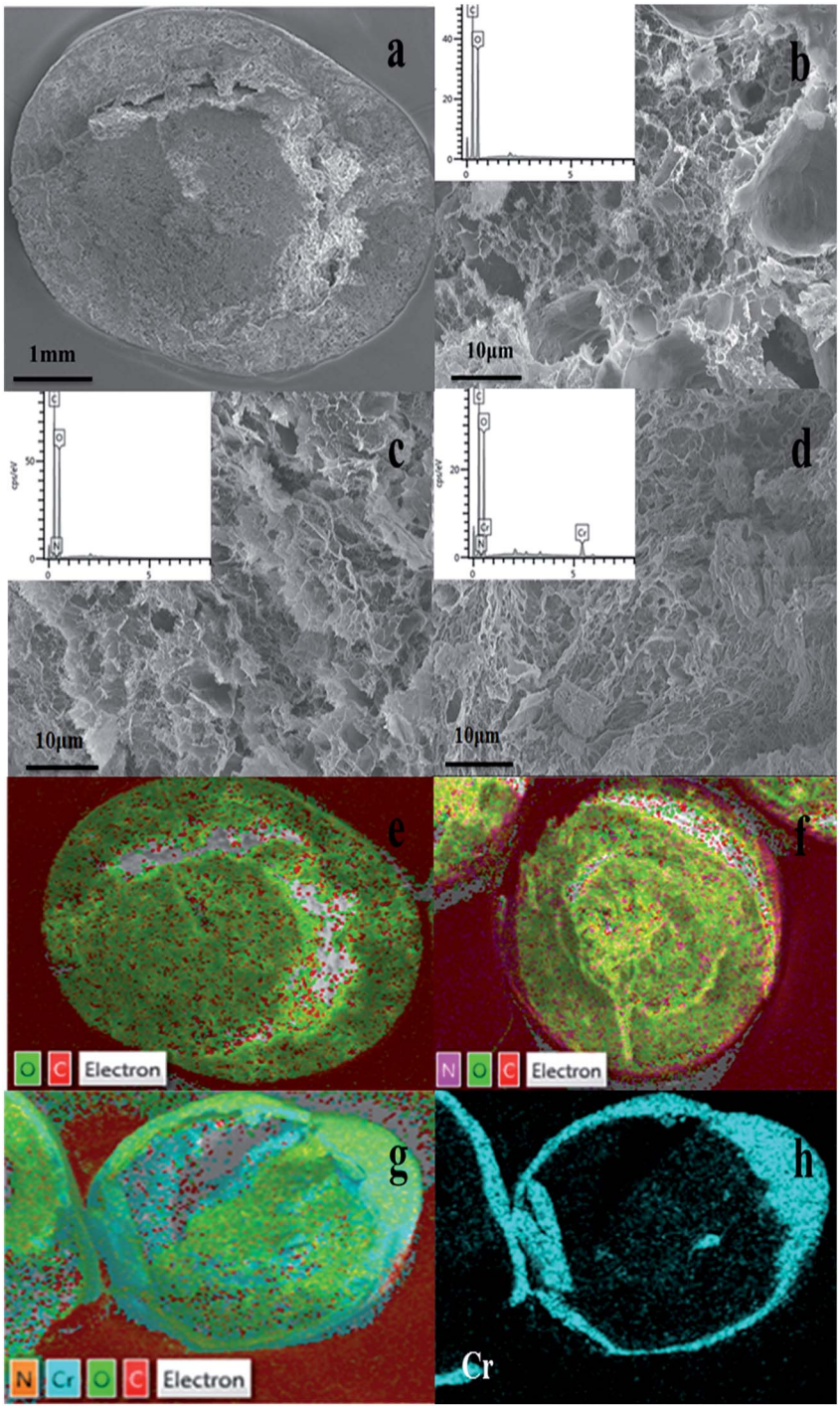

Fig. 8 SEM images of (a, b) CA, (c) CPA-2, (d) CPA-2-Cr; EDX pattern of (e) CA, (f) CPA-2, (g, h) CPA-2-Cr (insets show EDX pattern of element type and content of CA, CPA-2 and CPA-2-Cr).

was detected in CPA-2 (Fig. 8f). Given that there are amount of amino groups on PEI molecules, the existence of N element indicated that PEI had been grafted on CA beads resoundingly which was proved by the following XPS analysis. As depicted in Fig. 8g and h, the existence of Cr was obviously observed on the surface of CPA-2-Cr, demonstrating that Cr(VI) ions have been absorbed on the surface of adsorbent under testing conditions. In addition, other EDX spectra (Fig. 8b–d insets) clearly displayed the change of element type and content of CA, CPA-2 and CPA-2-Cr.

3.3.2 FTIR analysis. The functional groups of CA, CPA-2 and CPA-2-Cr were characterized by FTIR spectroscopy, and the typical spectra were shown in Fig. 8. The characteristic peaks of CA (Fig. 9a) appeared at 3444 cm^{-1} and 2921 cm^{-1}, belonging to the stretching vibrations of O–H and C–H bonds.[43] The adsorption peak at 1160 cm^{-1} corresponded to the C–O

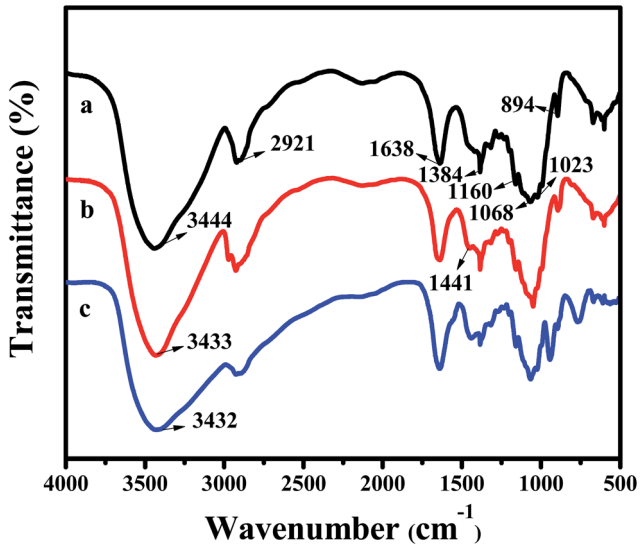

Fig. 9 FT-IR spectra of (a) CA, (b) CPA-2 and (c) CPA-2-Cr.

stretching vibrations. The bands at 1023 cm^{-1} and 1068 cm^{-1} were assigned to the C–O–C pyranose ring skeletal vibrations.[44] The peak located at 1638 cm^{-1} corresponded to the bending mode of absorbed water.[45] The band at 1384 cm^{-1} related to the bending vibrations of hydroxyl groups and the peak at 894 cm^{-1} may be attributed to the β-glucosidic linkages between the sugar units in cellulose.[46] After modification of porous cellulose with PEI, the broad peak at about 3400 cm^{-1} become wider and stronger in Fig. 9b, which could be assigned to the superposition of the stretching vibrations of O–H and N–H groups. Moreover, the new band appeared at 1441 cm^{-1} represented the C–N vibrations. These results confirmed that amino groups were introduced onto the cellulose surface and the adsorbent of core–shell/bead-like CPA-2 was successfully synthesized. In the spectrum of CPA-2-Cr (Fig. 9c), the adsorption peaks at 3400 cm^{-1} and 2920 cm^{-1} were weakened, indicating that the amino and hydroxyl groups of the surface of CPA-2 played an important role in the uptake process.

3.3.3 BET analysis. The relevant textural parameters of CA and CPA-2 calculated from nitrogen adsorption–desorption isotherms were summarized in Table S1.† It revealed that the BET surface area of CPA-2 (36.77 $m^2\ g^{-1}$) was slimly smaller than that of CA (41.7 $m^2\ g^{-1}$). The average pore sizes of CA and CPA-2 were approximately 13.7 and 13.5 nm, respectively. The results mentioned above are in agreement with SEM, and the most likely cause is that PEI molecules were grafted on CA hydrogels which blocked some pores, again suggesting that PEI

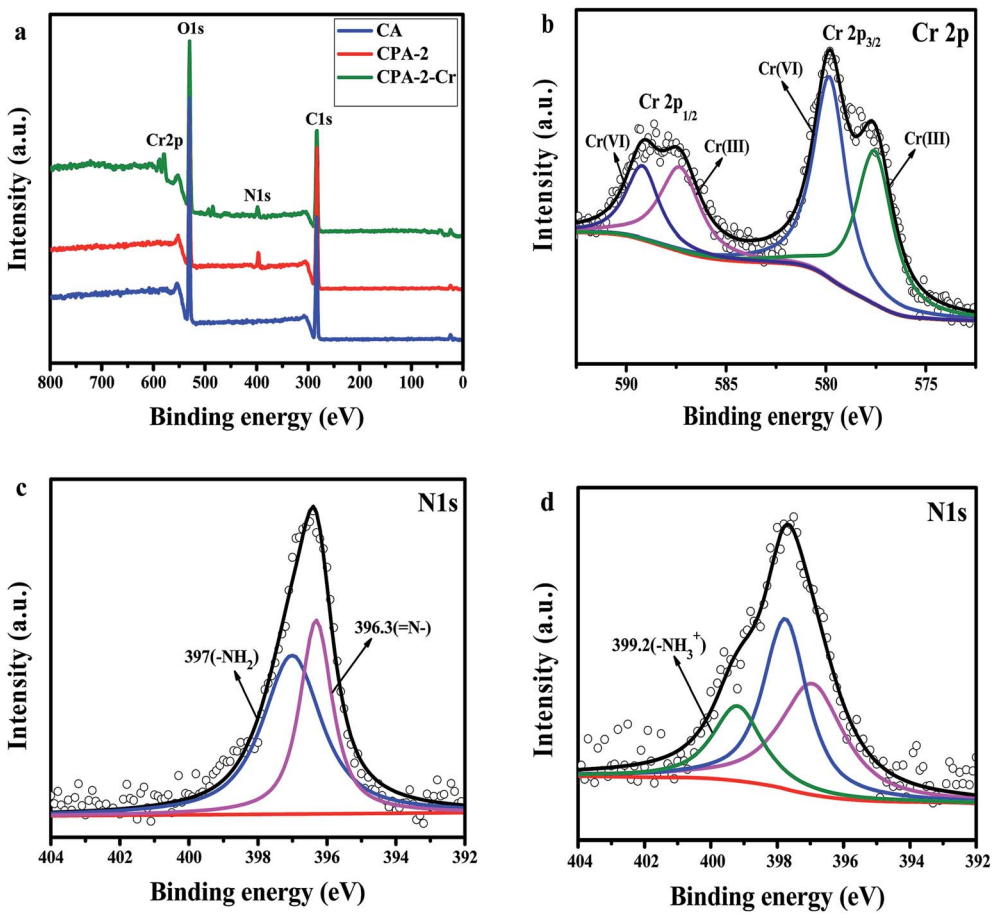

Fig. 10 XPS spectra of (a) total survey spectra of CA, CPA-2 and CPA-2-Cr, (b) Cr 2p spectrum of CPA-2-Cr, (c) N 1s spectra of CPA-2, (d) N 1s spectra of CPA-2-Cr.

had been successfully grafted onto CA. As seen in Fig. S2,† CA and CPA-2 exhibited a typical type IV curves with hysteresis loops, which is typical for mesopore material. The mesopore structure is favorable for mass transfer between sorbent and hexavalent chromium.

3.4 Adsorption mechanism over resultant sample

Through the pH effect study, it is known that the sorption process is regarded as the result of electrostatic interaction between protonated amine group ($-NH_3^+$) and Cr(VI) ions. For the advanced investigation of the adsorption mechanism, XPS spectra of CA, CPA-2 and CPA-2-Cr were studied and the spectra were shown in Fig. 10. As illustrated in the XPS total survey spectra (Fig. 10a), the photoelectron lines of CA at binding energies of about 285 and 533 eV were related to C 1s and O 1s, respectively. The existence of N element in the CPA-2 was demonstrated by the peak in the wide scan spectrum with binding energy at 400 eV. For the spectrum of CPA-2-Cr, there were two peaks at 579 and 588 eV appeared, which related to Cr $2p_{3/2}$ and Cr $2p_{1/2}$ orbits, respectively, demonstrating that Cr(VI) was successfully adsorbed by CPA-2. All these results were in accordance with the EDX and FTIR analyses. The high-resolution Cr 2p spectrum could be split into four peaks (Fig. 10b). The peaks at 577.6 eV (Cr $2p_{3/2}$) and 587.3 eV (Cr $2p_{1/2}$) were assigned to Cr(III) and the others at 579.8 eV (Cr $2p_{3/2}$) and 589.1 eV (Cr $2p_{1/2}$) were ascribed to Cr(VI), demonstrating that Cr(VI) and Cr(III) coexist on the porous surface of CPA-2.[47]

The removal of chromium was generally depended on the functional groups on the surface of sorbent. Fig. 10c and d displayed the N 1s spectra of CPA-2 before and after Cr(VI) adsorption. In Fig. 10c, the peaks at 396.3 and 397 eV were attributed to =N– and $-NH_2$, respectively. After adsorbing Cr(VI), as shown in Fig. 8d, the new peak appeared at 399.2 eV assigned to $-NH_3^+$, and the peaks of =N– and $-NH_2$ had corresponding shift, indicating that amino groups from PEI participated in the Cr(VI) removal process.

From the above analysis, the mechanism of Cr(VI) removal could be concluded as follows; on the one hand, the amino groups on the adsorbent could be effectively protonated to $-NH_3^+$ at lower pH, and Cr(VI) anions were adsorbed on CPA-2 *via* electrostatic attraction. On the other hand, Cr(VI) was reduced to less toxic Cr(III) by a redox reaction occurred between Cr(VI) and CPA-2. The existence of amino and hydroxyl groups acting as electron donors could be responsible for the reduction of Cr(VI) to Cr(III) during the adsorption process. Most of the Cr(III) immobilized on CPA-2 surface through ion exchange or surface complexation and a few of residual Cr(III) were released to solution again. The proposed removal mechanism was depicted in Scheme 2.

3.5 Regeneration studies

Desorption and regeneration experiments were designed to assess the practical utility of CPA-2, due to reusability is important for adsorbent to decrease economic cost. To do so,

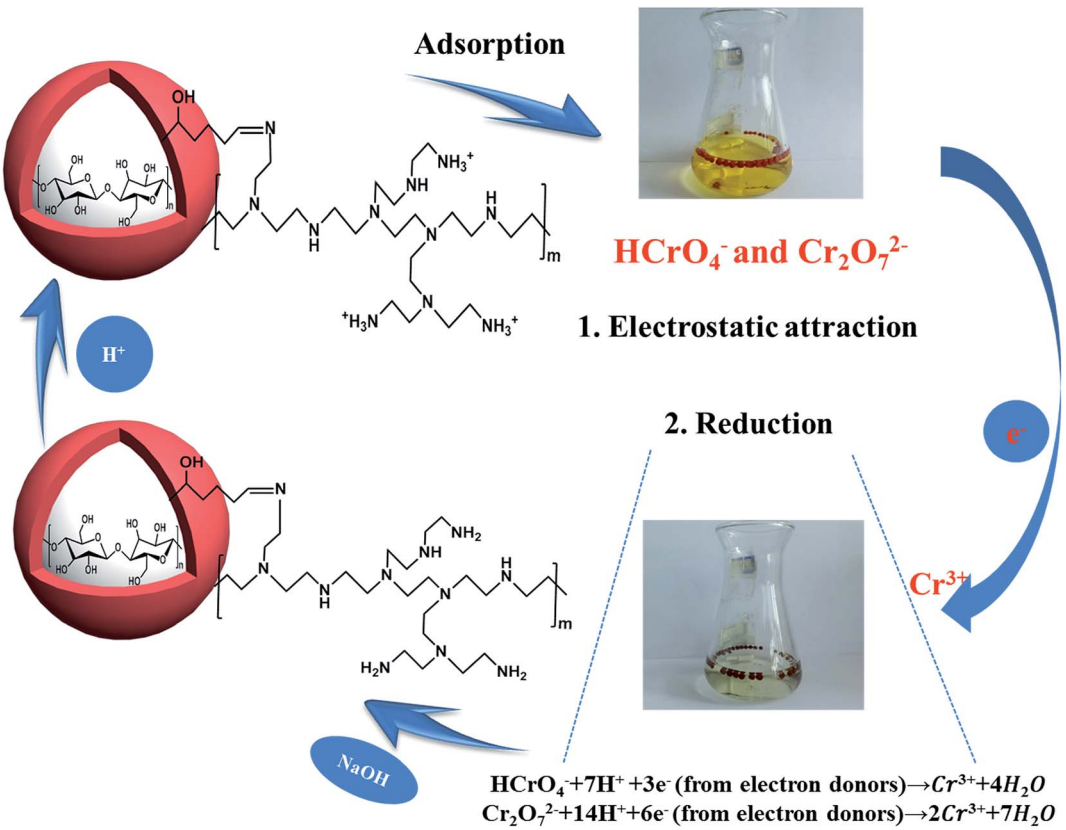

Scheme 2 The mechanism for the removal of Cr(VI) by CPA-2.

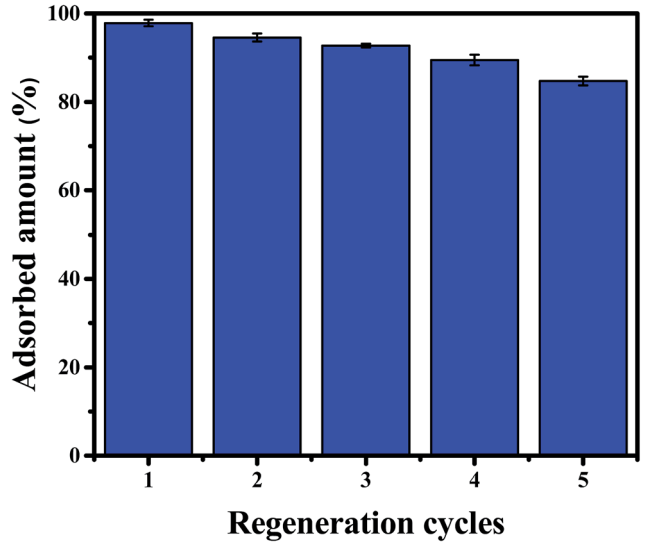

Fig. 11 The reusability of CPA-2 for the adsorption of Cr(VI).

0.02 g CPA-2 beads was added into 20 mL of 50 mg L^{-1} Cr(VI) solution by shaking at 180 rpm at 25 °C for 24 h. The Cr(VI)-adsorbed CPA-2 beads were collected and eluted for 30 min using 50 mL of a solution of 0.2 mol L^{-1} NaOH and 0.2 mol L^{-1} NaCl, and then rinsed with deionized water to pH 6–7 for reuse in the second run. After five adsorption–desorption cycles, the removal efficiency still kept above 80% (Fig. 11), indicating that CPA-2 beads could be repeatedly utilized in removing Cr(VI) from effluents. The decrease in adsorption capacity could be attributed to the loss of partial reduction property of CPA-2 and the unavoidable mass loss during the cyclic process.

4. Conclusion

In conclusion, a new type of low-cost, highly efficient, environmentally-friendly bead-like composite (CPA-2) was synthesized through cross-link reaction between the amine groups of PEI and the hydroxyl groups of cellulose, leading to the significant enhancement of Cr(VI) removal efficiency under batch and column systems. Either morphology analysis or changes of FTIR and XPS characteristic spectra demonstrated the successful modification of CPA-2 with PEI. The batch experimental results indicated that Cr(VI) adsorption capacity of CPA-2 was highly pH dependent, and the optimal pH value appeared at 2. The maximum adsorption capacity of CPA-2 was calculated to be 229.1 mg g^{-1}, which was much higher than previous reported adsorbents for Cr(VI) removal. Kinetics data suggested that the removal of Cr(VI) on CPA-2 fitted well with pseudo-second-order kinetic model while the equilibrium data were well described by Freundlich model. Column studies indicated that the adsorption of Cr(VI) on CPA-2 depended on flow rate and influent Cr(VI) concentration, and Thomas model was more suitable for the breakthrough curves of adsorption processes under different fixed-bed conditions. Mechanism investigations revealed that the removal of chromium by the CPA-2 was a complicated process, in which electrostatic interaction and a redox reaction were involved. More significantly, the CPA-2 beads could be easily separated and reused without significant loss of adsorption capacity even after five cycles. Generally speaking, as-prepared CPA-2 can be considered as a promising adsorptive material in the decontamination of chromium-polluted water.

Conflicts of interest

There are no conflicts to declare.

Acknowledgements

We acknowledge the financial support from the National Natural Science Foundation of China (21676039) and the Opening Foundation of State Key Laboratory of Inorganic Synthesis and Preparative Chemistry of Jilin University (2016-04) for this work.

References

1 H. Gu, S. Rapole, Y. Huang, D. Cao, Z. Luo, S. Wei and Z. Guo, *J. Mater. Chem. A*, 2013, **1**, 2011–2021.
2 R. Anderson, *Regul. Toxicol. Pharmacol.*, 1997, **26**, S35–S41.
3 W. Zheng, Q. An, Z. Lei, Z. Xiao, S. Zhai and Q. Liu, *RSC Adv.*, 2016, **6**, 104897–104910.
4 X. Lv, J. Xu, G. Jiang, J. Tang and X. Xu, *J. Colloid Interface Sci.*, 2012, **369**, 460–469.
5 T. Liu, Z. Wang, L. Zhao and X. Yang, *Chem. Eng. J.*, 2012, **189**, 196–202.
6 L. Keith, *Environ. Sci. Technol.*, 1979, **13**, 416–423.
7 S. Rengaraj, C. Joo, Y. Kim and J. Yi, *J. Hazard. Mater.*, 2003, **102**, 257–275.
8 R. Goyal, N. Jayakumar and M. Hashim, *J. Hazard. Mater.*, 2011, **195**, 383–390.
9 J. Dui, G. Zhu and S. Zhou, *ACS Appl. Mater. Interfaces*, 2013, **5**, 10081–10089.
10 P. Hu, X. Liang, M. Yaseen, X. Sun, Z. Tong, Z. Zhao and Z. Zhao, *Chem. Eng. J.*, 2018, **332**, 608–618.
11 L. Lin, S. Zhai, Z. Xiao, Y. Song, Q. An and X. Song, *Bioresour. Technol.*, 2013, **136**, 437–443.
12 L. Zhang, W. Xia, X. Liu and W. Zhang, *J. Mater. Chem. A*, 2015, **3**, 331–340.
13 X. Lei, X. Xue and H. Yang, *Appl. Surf. Sci.*, 2014, **321**, 396–403.
14 B. Saha and C. Orvig, *Coord. Chem. Rev.*, 2010, **254**, 2959–2972.
15 A. Albadarin, C. Mangwandi, A. Al-Muhtaseb, G. Walker, S. Allen and M. Ahmad, *Chem. Eng. J.*, 2012, **179**, 193–202.
16 D. Mulange Wa Mulange and A. Garbers-Craig, *J. Hazard. Mater.*, 2012, **223–224**, 46–52.
17 Y. Fan, R. Yang, Z. Lei, N. Liu, J. Lv, S. Zhai, B. Zhai and L. Wang, *Korean J. Chem. Eng.*, 2016, **33**, 1416–1424.
18 A. Kumar, S. Kalidhasan, V. Rajesh and N. Rajesh, *Ind. Eng. Chem. Res.*, 2012, **51**, 58–69.
19 B. Adhikari, M. Gurung, S. Alam, B. Tolnai and K. Lnoue, *Chem. Eng. J.*, 2013, **231**, 190–197.

20 Y. Yan, Q. An, Z. Xiao, W. Zheng and S. Zhai, *Chem. Eng. J.*, 2017, **313**, 475–486.
21 R. Li, Q. An, Z. Xiao, B. Zhai and S. Zhai, *RSC Adv.*, 2017, **7**, 40227–40236.
22 C. Liu, R. Jin, X. Ouyang and Y. Wang, *Appl. Surf. Sci.*, 2017, **408**, 77–87.
23 H. Qiao, Y. Zhou, F. Yu, E. Wang, Y. Min, Q. Huang, L. Pang and T. Ma, *Chemosphere*, 2015, **141**, 297–303.
24 X. Xiong, J. Duan, W. Zou, X. He and W. Zheng, *J. Membr. Sci.*, 2010, **363**, 96–102.
25 L. Zhao and H. Mitomo, *J. Appl. Polym. Sci.*, 2008, **110**, 1388–1395.
26 Y. Zhao, H. Shen, S. Pan, M. Hu and Q. Xia, *J. Mater. Sci.*, 2010, **45**, 5291–5301.
27 X. Tian, W. Wang, Y. Wang, S. Komarneni and C. Yang, *Microporous Mesoporous Mater.*, 2015, **207**, 46–52.
28 B. Chen, X. Zhao, Y. Liu, B. Xu and X. Pan, *RSC Adv.*, 2015, **5**, 1398–1405.
29 Y. Pang, G. Zeng, L. Tang, Y. Zhang, Y. Liu, X. Lei, Z. Li, J. Zhang, Z. Liu and Y. Xiong, *Chem. Eng. J.*, 2011, **175**, 222–227.
30 A. Donia, A. Atia and F. Abouzayed, *Chem. Eng. J.*, 2012, **191**, 22–30.
31 G. Bayramoğlu and M. Arica, *Chem. Eng. J.*, 2008, **139**, 20–28.
32 G. Zhao, J. Li, X. Ren, C. Chen and X. Wang, *Environ. Sci. Technol.*, 2011, **45**, 10454–10462.
33 X. Sun, Y. Ma, X. Liu, S. Wang, B. Gao and X. Li, *Water Res.*, 2010, **44**, 2517–2524.
34 Q. Cao, F. Huang, Z. Zhuang and Z. Lin, *Nanoscale*, 2012, **4**, 2423–2430.
35 R. Yu, Y. Shi, D. Yang, Y. Liu, J. Qu and Z. Z. Yu, *ACS Appl. Mater. Interfaces*, 2017, **9**, 21809–21819.
36 D. Setyono and S. Valiyaveettil, *J. Hazard. Mater.*, 2016, **302**, 120–128.
37 X. Sun, L. Yang, Q. Li, Z. Liu, T. Dong and H. Liu, *Chem. Eng. J.*, 2015, **262**, 101–108.
38 L. Zhuang, Q. Li, J. Chen, B. Ma and S. Chen, *Chem. Eng. J.*, 2014, **253**, 24–33.
39 J. Goel, K. Kadirvelu, C. Rajagopal and V. Garg, *J. Hazard. Mater.*, 2005, **125**, 211–220.
40 Q. Li, X. Tang, Y. Sun and H. Xu, *RSC Adv.*, 2015, **5**, 25337–25347.
41 H. Thomas, *J. Am. Chem. Soc.*, 1944, **66**, 1664–1666.
42 Y. Liu, G. Zhong, Z. Liu, M. Meng, Y. Jiang, L. Ni, W. Guo and F. Liu, *RSC Adv.*, 2015, **5**, 85691–85704.
43 L. Yun, H. Liu, R. Gao, S. Xiao, Z. Ming, Y. Yin, S. Wang, L. Jian and D. Yang, *ACS Appl. Mater. Interfaces*, 2016, **8**, 29179–29185.
44 J. Sun, X. Sun, H. Zhao and R. Sun, *Polym. Degrad. Stab.*, 2004, **84**, 331–339.
45 W. Li, A. Jin, C. Liu, R. Sun, A. Zhang and J. Kennedy, *Carbohydr. Polym.*, 2009, **78**, 389–395.
46 Z. Du, T. Zheng, P. Wang, L. Hao and Y. Wang, *Bioresour. Technol.*, 2016, **201**, 41–49.
47 H. Liang, X. Cao, W. Zhang, H. Lin, F. Zhou, L. Chen and S. Yu, *Adv. Funct. Mater.*, 2011, **21**, 3851–3858.
48 Y. Pang, G. Zeng, L. Tang, Y. Zhang, Y. Liu, X. Lei, Z. Li, J. Zhang, Z. Liu and Y. Xiong, *Chem. Eng. J.*, 2011, **175**, 222–227.
49 S. Babel and T. Kurniawan, *Chemosphere*, 2004, **54**, 951–967.
50 K. Low, C. Lee and A. Ng, *J. Environ. Sci. Health, Part A: Environ. Sci. Eng. Toxic Hazard. Subst. Control*, 1997, **23**, 1849–1860.
51 J. Li, X. Miao, Y. Hao, J. Zhao, X. Sun and L. Wang, *J. Colloid Interface Sci.*, 2008, **318**, 309–314.
52 X. Sun, L. Yang, Q. Li, J. Zhao, X. Li, X. Wang and H. Liu, *Chem. Eng. J.*, 2014, **241**, 175–183.
53 L. Li, L. Fan, M. Sun, H. Qiu, X. Li, H. Duan and C. Luo, *Colloids Surf., B*, 2013, **107**, 76–83.